AGU100 ADVANCING EARTH AND SPACE SCIENCE

JGR Biogeosciences

RESEARCH ARTICLE
10.1029/2019JG005464

Special Section:
Carbon cycling in tidal wetlands and estuaries of the contiguous United States

Controls on Sediment Accretion and Blue Carbon Burial in Tidal Saline Wetlands: Insights From the Oregon Coast, USA

Erin K. Peck[1], Robert A. Wheatcroft[1], and Laura S. Brophy[1,2]

[1]College of Earth, Ocean, and Atmospheric Sciences, Oregon State University, Corvallis, OR, USA, [2]Institute for Applied Ecology, Corvallis, OR, USA

Key Points:
- Oregon tidal saline wetlands kept pace with twentieth-century sea level rise, except in the central coast, the reasons for which are unclear
- In estuaries with a positive accretionary balance, both sea level rise and sediment load relative to estuary area control accretion
- Blue carbon burial rates, provided herein, are the first such measurements for Oregon tidal saline wetlands

Supporting Information:
- Supporting Information S1
- Figure S1
- Figure S2

Correspondence to:
E. K. Peck,
peckerin@oregonstate.edu

Citation:
Peck, E. K., Wheatcroft, R. A., & Brophy, L. S. (2020). Controls on sediment accretion and blue carbon burial in tidal saline wetlands: Insights from the Oregon coast, USA. *Journal of Geophysical Research: Biogeosciences*, *125*, e2019JG005464. https://doi.org/10.1029/2019JG005464

Received 6 SEP 2019
Accepted 25 JAN 2020
Accepted article online 2 FEB 2020

Abstract Oregon estuaries provide important opportunities to assess controls on tidal saline wetland carbon burial and sediment accretion as both rates of relative sea level rise (RSLR; -1.4 ± 0.9 to 2.8 ± 0.8 mm yr^{-1}) and fluvial suspended sediment load relative to estuary area (0.23 to 17×10^3 t km^{-2} yr^{-1}) vary along the coast. We hypothesized that vertical accretion, measured using excess ^{210}Pb in least-disturbed wetlands within seven Oregon estuaries, would vary with either RSLR or sediment load relative to estuary area, and carbon burial would correlate strongly to sediment accretion. Mean rates of high marsh accretion (0.8 ± 0.2 to 4.1 ± 0.2 mm yr^{-1}) indicate that Oregon tidal wetlands have mainly kept pace with twentieth-century RSLR with the exception that the accretionary balance in the central coast is negative, suggesting drowning. Experiencing the fastest rates of RSLR, central-coast estuaries may foreshadow the fates of other Oregon estuaries under future accelerated sea level rise. Comparison of mass accumulation rates with sediment loads, however, indicates low trapping efficiency and therefore no fluvial sediment limitation. Thus, nonlinear feedback between RSLR and sediment accretion may enhance wetland resistance to drowning. Among wetlands keeping pace with or exceeding RSLR, sediment accretion displays no significant relationship with elevation but rather appears controlled by both the rate of RSLR and relative sediment load, highlighting the importance of incorporating both factors into future studies of tidal saline wetlands. Carbon burial rates, controlled by sediment accretion, will likely increase with future accelerated sea level rise.

Plain Language Summary Salt marshes and brackish scrub-shrub and forested tidal wetlands, collectively known as tidal saline wetlands, provide valuable services such as habitat for wildlife, protection from coastal flooding, and carbon sequestration. Despite their importance, tidal saline wetlands are threatened by sea level rise and scientists must better understand what controls their growth so as to make predictions of their future survival. Additionally, sediment accumulation within tidal saline wetlands is an important control on the amount of carbon sequestered in coastal areas; thus, understanding how these systems will evolve in the coming decades may shed light on the global carbon cycle and climate change. New results from the Oregon coast indicate that both the local pace of sea level rise and the amount of sediment delivered by rivers control tidal saline wetland growth. Because sea level rise is relatively slow in Oregon and Pacific Northwest rivers deliver relatively high amounts of sediment to the coast, Oregon tidal saline wetlands may be resistant to future drowning. However, of the seven estuaries studied, two showed evidence of drowning over the last century; the reasons for this are unclear but may relate to the local pace of sea level rise or other processes not accounted for in this study.

1. Introduction

Tidal wetlands maintain high biotic diversity and primary productivity (Beck et al., 2001), influence biogeochemical cycles as a critical junction between terrestrial and marine environments (Turner & Millward, 2002), and are considered some of the most valuable ecosystems on the planet (Barbier et al., 2011). Tidal wetlands are responsible for 50% of marine carbon (so called "blue carbon") burial, despite occupying only 0.2% of the ocean surface (Duarte et al., 2013), highlighting the importance of these systems to the global carbon cycle (Windham-Myers et al., 2019, and references within). However, half of all tidal wetlands have already been lost or degraded globally (Barbier et al., 2011), and another 1 to 2% (by area) are estimated to be lost each year (Pendleton et al., 2012). Approximately 85% of U.S. West Coast vegetated tidal wetlands

have already been lost (Brophy et al., 2019), and under high sea level rise rates, 83% of current West Coast tidal saline wetlands are projected to fully submerge by 2110 (Thorne et al., 2018). Despite their clear importance and possible threatened status, these systems are influenced by complex ecogeomorphic feedback, and questions related to tidal saline wetland morphodynamics remain. Oregon estuaries present compelling opportunities to expand our understanding of tidal saline wetland sediment accumulation and blue carbon burial and thus shed light on estuarine morphodynamics globally.

Oregon estuaries are understudied and therefore underrepresented within literature concerning blue carbon burial and global wetland change (e.g., Chmura et al., 2003; Crosby et al., 2016; Kirwan, Temmerman, et al., 2016; Morris et al., 2016; Ouyang & Lee, 2014). Indeed, although there exists considerable variation in tectonic, geomorphic, and anthropogenic settings along the U.S. West Coast, California data frequently represent the entire coast in comparative studies. Thom (1992) published some of the first vertical accretion rates measured within Oregon tidal saline wetlands. This preliminary study obtained a limited number ($n = 2$) of ^{137}Cs-derived vertical accretion rates within the Salmon River Estuary. Thorne et al. (2018) recently expanded the regional data set by measuring tidal saline wetland accretion rates using ^{137}Cs within three Oregon estuaries—Siletz Bay ($n = 3$), Coos Bay ($n = 3$), and Coquille River Estuary ($n = 3$). Considering the complexity within and among estuaries, a primary motivation of our study is to provide more comprehensive sediment accretion rate data for undisturbed tidal saline wetlands in Oregon. Moreover, to our knowledge, no previous study has quantified carbon burial within Oregon tidal saline wetlands.

As an additional motivation, our study of Oregon tidal saline wetlands may provide data unique to global compilations of wetland change. For instance, Oregon tidal saline wetlands may serve as end-members in global assessments of marsh vulnerability to relative sea level rise (RSLR). In recently published compilations, Kirwan, Temmerman, et al. (2016) and Crosby et al. (2016) examined instances of salt marsh accretion rates compared with RSLR rates primarily above 1 mm yr^{-1}. The range of relative sea level change within Oregon estuaries extends as low as −1.5 mm yr^{-1} (Komar et al., 2011). Also, some have contended that bias within the literature toward reporting predominantly on threatened tidal wetlands has led to an exaggeration of wetland vulnerability to RSLR acceleration (Kirwan, Temmerman, et al., 2016). As a region that experiences negative to low rates of RSLR (Komar et al., 2011), an abundance of fluvial suspended sediment (Wheatcroft & Sommerfield, 2005), and limited human alteration (Thom & Borde, 1998), additional Oregon data would therefore contribute new examples to global compilations.

Perhaps most compellingly, quantification of organic and inorganic sediment accretion could help constrain the relative impacts of sea level change and sediment delivery rates on tidal wetland evolution. Redfield (1972) was one of the first to elucidate the balance between available sediment and RSLR in tidal wetland accretion; since then, RSLR has traditionally been thought to control the formation and evolution of tidal wetlands given no limitation of suspended sediment (Friedrichs & Perry, 2001). As relative sea level rises, creating accommodation space, the wetland platform aggrades vertically through nonlinear feedback between the vegetation, sediment, and estuarine flow field, thereby maintaining position relative to sea level. However, recent studies have indicated that changes in sediment delivery rates may have largely determined the behavior of estuaries along the Atlantic and Gulf coasts of North America (e.g., Colman & Bratton, 2003; Day et al., 2000; Gunnell et al., 2013; Kirwan et al., 2011). Following accelerated downstream sediment delivery due to erosion, often associated with land use change, and subsequent expansion of tidal wetlands, ecogeomorphic feedback maintain estuarine morphology after sediment supply slows. Whether organic and inorganic accretion within tidal wetlands is primarily influenced by RSLR or by fluvial sediment flux remains uncertain.

Oregon estuaries present an opportunity to constrain the relative impacts of sea level change and sediment delivery rates over the past ~100 years because both factors vary along the coast, but in relatively well understood ways. Vertical land motions at the Oregon coast result from the large-scale subduction of the Juan de Fuca plate underneath the North American plate, and trench-parallel differences in strain accumulation cause latitudinally varying uplift rates (Mitchell et al., 1994). Eustatic sea level rise (ESLR) in the Northeast Pacific Ocean coupled with variable uplift results in relative sea level changes between −1.5 mm yr^{-1} in southern and northern Oregon (i.e., falling relative sea level), and rises of +2 mm yr^{-1} in central Oregon (Komar et al., 2011). Independently, there exists a roughly 30-fold range in fluvial sediment flux to Oregon estuaries due primarily to variations in river basin area (Wheatcroft & Sommerfield, 2005).

Table 1
Estuary Characteristics; Estimates of Relative Sea Level Rise (RSLR), Calculated Using the Average Uplift Rate and Eustatic Sea Level Rise (ESLR); and Sediment Loads for Each Estuary

	Youngs	Nehalem	Tillamook	Netarts	Salmon	Alsea	Coquille
Watershed area (km^2)	161	2209	1336	42	193	1221	2736
Historic estuary area (km^2)	22.9	21.3	56.8	10.7	3.57	14.4	43.8
Current estuary area (km^2)	9.03	14.8	38.8	10.6	3.32	13.1	10.4
Current tidal wetland area (km^2)	2.81	5.47	4.94	1.20	2.30	3.67	1.57
MTL (m)	1.42	1.37	1.37	1.09	1.13	1.24	1.15
MHHW (m)	2.68	2.60	2.54	2.09	2.17	2.31	2.16
ESLR (mm yr^{-1})	2.5 ± 1.1	2.9 ± 1.0	3.0 ± 1.0	3.1 ± 1.0	3.4 ± 0.9	3.5 ± 0.8	1.9 ± 0.9
Mean uplift (mm yr^{-1})	2.2 ± 0.1	1.9 ± 0.1	1.2 ± 0.1	1.6 ± 0.0	1.2 ± 0.0	0.7 ± 0.0	3.3 ± 0.0
RSLR (mm yr^{-1})	0.3 ± 1.1	0.9 ± 1.0	1.9 ± 1.0	1.5 ± 1.0	2.2 ± 0.9	2.8 ± 0.8	−1.4 ± 0.9
Sediment load ($\times 10^3$ t yr^{-1})	26.8	224	245	2.5	20.1	110	178
Relative sediment load ($\times 10^3$ t km^{-2} yr^{-1})	3.0	15	6.3	0.23	6.1	8.4	17

Note. Historic (includes currently diked areas) and current (excludes currently diked areas) estuary areas and current tidal wetland areas were estimated using the Pacific Marine and Estuarine Fish Habitat Partnership (PMEP)'s West Coast USA Estuarine Biotic Habitat maps (Brophy et al., 2019). Mean tide level (MTL) and MHHW are expressed relative to MLLW based on NOAA tidal datums. The standard deviations of the uplift rates and ESLR errors were used in calculating RSLR error by standard error propagation laws. Loads were additionally estimated for the seven estuaries using the USGS SPARROW model (Wise, 2018). Watershed area for Youngs River Estuary and Tillamook Bay exclude the Lewis and Clark River and the Miami River, respectively. Because the load values are modeled approximations, no error was estimated. Relative sediment load was calculated by dividing sediment load by current estuary area.

Secondary variables, including tidal range, water temperature and salinity patterns, and tectonic history (Hickey & Banas, 2003; Kemp et al., 2018), are similar among these estuaries.

To examine these topics, we measured vertical accretion and carbon burial rates using excess ^{210}Pb and C_{org} data along elevation gradients within scrub-shrub tidal wetlands, high marsh, low marsh, and mudflats of seven Oregon estuaries that vary in RSLR and fluvial sediment flux: Youngs River Estuary, Nehalem Bay, Tillamook Bay, Netarts Bay, Salmon River Estuary, Alsea Bay, and Coquille River Estuary. This assessment will fill critical knowledge gaps, providing an estimate of whether these ecosystems were resilient to anthropogenic and climatic stresses over the last century and contributing to global compilations of wetland change. Moreover, comparison of these accretion values to rates of RSLR and fluvial sediment load may allow us to better constrain which physical drivers predominately control tidal wetland growth.

2. Methods

2.1. Study Settings

Estuaries were selected to span a range of RSLR rates and fluvial sediment supply. Although both RSLR and sediment supply differ along the Oregon margin, these seven estuaries share many similar secondary characteristics, such as water temperature, mean annual precipitation, watershed relief, and semidiurnal tide ranges (Hickey & Banas, 2003). Additionally, although the degree varies, these estuaries have similar histories of diking, primarily for grazing and other agriculture, as evidenced by the difference in historic and current estuary extents (Table 1).

Four tidal saline wetland classes were sampled: scrub-shrub tidal wetlands, high marsh, low marsh, and mudflats (see Table S1 for dominant plant species for each sampled wetland class). The scrub-shrub wetlands were vegetated by a dense herbaceous layer of graminoids (grass-like plants), plus overhanging shrub canopy. Similarly dense graminoid vegetation with little to no bare ground characterizes high marsh in these estuaries. The low marsh sites were dominated by low-growing, halophytic species, often succulents; bare ground was often present. Mudflats were unvegetated.

Rates of ESLR were combined with mean uplift rates to yield estuary-specific RSLR rates (Table 1). Although others have employed a single value for ESLR along the entire PNW coast in calculating relative sea level change (e.g., Komar et al., 2011), we have determined regionally specific ESLR estimates to produce moderately more refined rates. Values of ESLR were taken from Mazzotti et al. (2008), who calculated the rates by deriving precise relative sea level change rates and GPS-derived vertical velocities for tide gauges along the PNW coast; these rates were verified with 1993–2003 satellite altimetry. The Astoria (OR) tide gauge, located

in the lower Columbia River, provided the rate of ESLR for Youngs River Estuary. Because Nehalem Bay, Tillamook Bay, Netarts Bay, and Salmon River Estuary lie between the Astoria and South Beach (OR) gauges, a linear relationship between latitude and ESLR was used to estimate rates for these estuaries. The rates for Alsea Bay and Coquille River Estuary were estimated using linear relationships between the ESLR rates for the South Beach and Charleston (OR) gauges, and the Charleston and Crescent City (CA) gauges, respectively. Due to subduction of the Juan de Fuca plate beneath the North American plate, interseismic uplift is variable along the Cascade margin (Mazzotti et al., 2008). Benchmark uplift rates, provided in the Burgette et al.'s (2009) supporting information, were interpolated using natural neighbor interpolation for the seven estuaries (Table 1). These values were consistent with those published for the Astoria and South Beach NOAA tide gauges by Mazzotti et al. (2008).

Total suspended sediment loads were estimated for the contributing rivers and streams of each estuary using the U.S. Geological Survey's SPAtially Referenced Regressions On Watershed attributes (SPARROW) model for Western Oregon (Wise, 2018; Wise & O'Connor, 2016). Load estimates included contributions from the major rivers, small streams, and shoreline runoff. Because sites within Youngs River Estuary are located on the Youngs River, we distinguish this area from the greater Youngs Bay, and suspended sediment load contributed by the Lewis and Clark River was not included in the estimate. Additionally, the sediment contribution from the Miami River was not included in the estimated load for the Tillamook sites because that river discharges much nearer to the estuary's mouth. Suspended sediment loads relative to estuary area, hereby termed “relative sediment loads,” were calculated for comparison between estuaries.

2.2. Field Collection

Between 2010 and 2018, 72 sediment cores were collected from the intertidal zones of least-disturbed tidal saline wetlands from seven estuaries along the Oregon coast (Figure 1). Core locations were chosen at random using a three-stage process: (1) using GIS, estuaries were stratified by wetland type (scrub-shrub, high marsh, low marsh, and mudflat) defined by elevation from LIDAR digital elevation models and dominant vegetation; (2) target core locations (coordinates) were placed in homogeneous areas at approximately the center of each stratum; and (3) in the field, handheld consumer-grade GPS was used to randomly determine the final core location as the GPS introduced ≤5 m of random error to the true location. Scrub-shrub was defined as tidal wetland above mean higher high water (MHHW) dominated by woody plants less than 6 m tall (Cowardin et al., 1979). High marsh was defined as tidal wetland above MHHW and dominated by herbaceous species previously described as typical of high marsh (Janousek et al., 2019; Janousek & Folger, 2014; Jefferson, 1975). Low marsh was defined as tidal wetland below MHHW and dominated by herbaceous species previously described as typical of low marsh (Janousek et al., 2019; Janousek & Folger, 2014; Jefferson, 1975). Cores were preferentially collected within the high marsh because this wetland type is found at an elevation most often considered to be in equilibrium with RSLR and covers a greater areal extent than low marsh in Oregon estuaries. High marsh cores also frequently provide the clearest accumulation rate data. Selected locations likely to have aberrant depositional regimes (e.g., on channel banks or in swales) were excluded, as were sites that were known to have been fully diked. PVC pipes that were 10 cm in diameter and either 1.5 or 3 m in length were driven into the wetland using a sledgehammer. Compaction was estimated by measuring the depth from the top of the PVC pipe to the sediment surface both inside and outside of the core. Core compaction averaged 15 ± 8 cm, which corresponded to a mean of 6.7 ± 3.8% over the entire core length. Each core was then sealed at the sediment surface with a test plug and extracted with a truck jack. Elevation estimates of the sediment surface were made using a Real-Time Kinematic GPS, which returned an accuracy of 5 cm or better (generally 1–2 cm). To compare between sites, standardized elevations (z^*) were calculated as (elevation − mean tide level)/(mean higher high water − mean tide level) (Swanson et al., 2014).

2.3. Sediment Analyses

Computed tomography (CT) imaging provides nondestructive, high-resolution, three-dimensional views of stratigraphy that include physical and biogenic sedimentary structures, plant material, and potential artifacts. Within a week after collection, all core sections were scanned at 0.5-mm resolution using a Toshiba Aquilion 64-slice CT unit (Figure S1). Because X-ray attenuation primarily varies with the density of a material, X-radiography is particularly useful in quantifying sediment bulk density (Davey et al., 2011; Wheatcroft et al., 2006). To calculate dry bulk density (ρ_{DB}) throughout the sediment cores, we

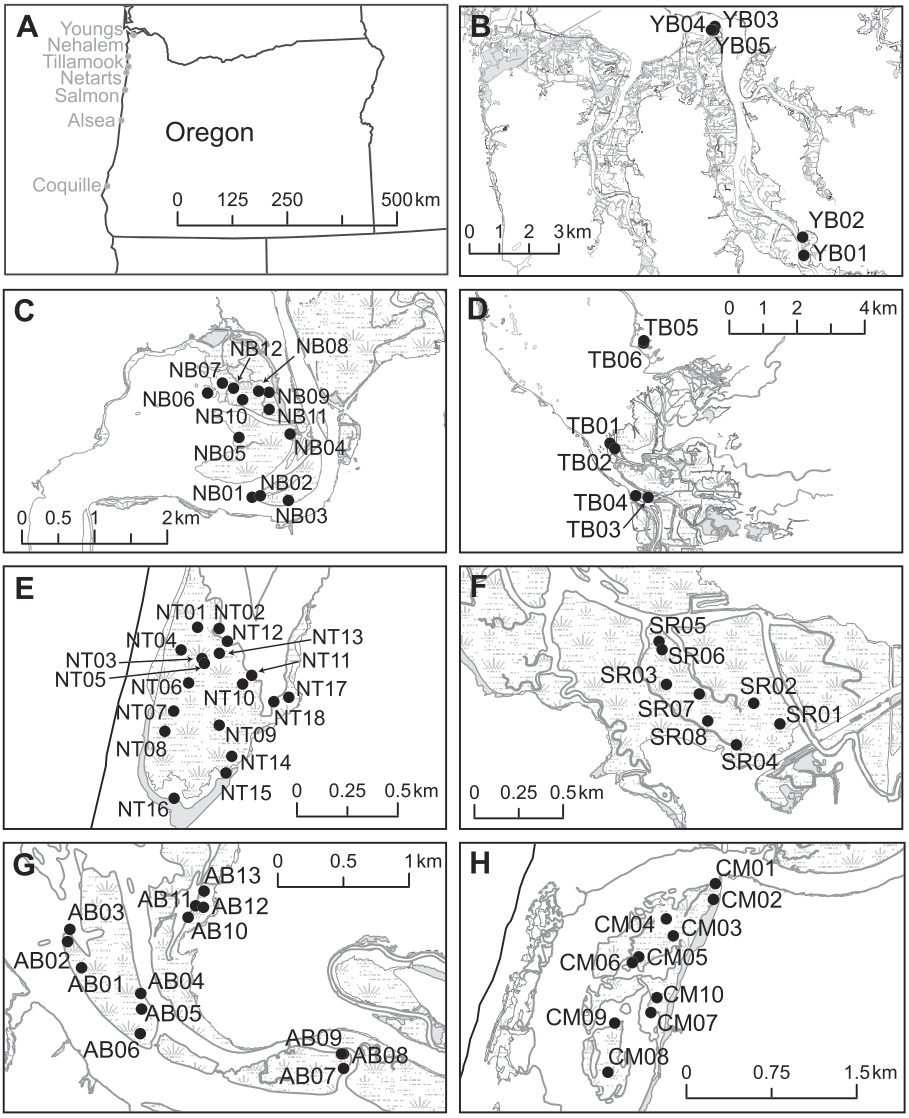

Figure 1. Maps depicting core locations within the tidal wetlands of each estuary. Maps were created using Pacific Marine & Estuarine Fish Habitat Partnership (PMEP)'s West Coast, USA. Estuarine Biotic Habitat maps (Brophy et al., 2019). High and low marshes are displayed as light gray marsh pattern and scrub-shrub and forested wetlands are displayed as solid gray. (a–h) Oregon coast, Youngs River Estuary, Nehalem Bay, Tillamook Bay, Netarts Bay, Salmon River Estuary, Alsea Bay, and Coquille River Estuary. Coordinates are provided in Table S1.

determined a relationship between CT-derived grayscale values and independently determined ρ_{DB} (Fourqurean et al., 2014) on a subset of samples (n = 829). These data were binned into 10 bins to account for differing sampling volumes between these two methods; a single ρ_{DB} measurement was collected within each 2-cm depth interval, whereas CT grayscale was measured at every 0.5-mm depth interval and averaged over each 2 cm.

Sediment cores were split length-wise, sampled at 2-cm increments, and freeze-dried. Large plant material was removed with forceps, and the dried sediment was ground to a consistent texture using a mortar and pestle. Samples were analyzed for percent organic matter (OM) at 2-cm increments to 50 cm by a standard loss-on-ignition (LOI) technique as recommended by Heiri et al. (2001). To calculate C_{org} in all samples from the OM data, LOI-derived OM was correlated with C_{org} by measuring a representative subset of samples by elemental analysis (n = 66; e.g., Goñi & Thomas, 2000). Mean sediment C_{org} density (g C_{org} cm^{-3}) was calculated for the top 50 cm of each core as the product of mean ρ_{DB} and mean C_{org} content.

2.4. Radionuclide Analysis

Samples were prepared for γ-ray spectroscopy by placing dried, disaggregated sediment in polystyrene counting jars. Samples were counted for ≥24 hr on two essentially identical Canberra GL2020RS LEGe planar γ-ray spectrometers (Wheatcroft et al., 2013). The ^{210}Pb and ^{214}Pb activities were measured at 46.5- and 351.9-keV photopeaks, respectively, to calculate excess ^{210}Pb activities, and ^{137}Cs was measured using the 661.6-keV photopeak. Samples were counted downcore until extinction of both radionuclides below the detection limit (3 Bq kg^{-1}).

Sediment accumulation rate (SAR) was calculated using the constant initial concentration (CIC) model (e.g., Sanchez-Cabeza & Ruiz-Fernández, 2012; Wheatcroft et al., 2013) applied to the excess ^{210}Pb activities (Figure S2; Ritchie & McHenry, 1990). The CIC method was chosen over other models for analyzing excess ^{210}Pb-derived accumulation rates, specifically the constant-flux-constant sedimentation or constant rate of supply models, as it is a straightforward and widely used model (e.g., Callaway et al., 2012; Mudd et al., 2009). Based on the downcore profiles of excess ^{210}Pb decay (Figure S2), it seems that the assumptions of the CIC model, specifically that the initial excess ^{210}Pb activity at the sediment surface is constant and that excess ^{210}Pb activity monotonically decreases with depth (Arias-Ortiz et al., 2018), are met.

Mass accumulation rate (g m^{-2} yr^{-1}) was calculated by the CIC model using mass depth (g m^{-2}; Sanchez-Cabeza & Ruiz-Fernández, 2012), and carbon mass accumulation rate (CAR; g C_{org} m^{-2} yr^{-1}) was calculated using C_{org} mass depth (g C_{org} m^{-2}). Error for each accumulation rate was calculated as the standard error of each regression (Table S1).

In accordance with best practices for reporting reproducible excess ^{210}Pb-derived accumulation rates (Mustaphi et al., 2019), all relevant data are maintained by the Smithsonian Environmental Research Center's Coastal Carbon Research Coordination Network and available at doi.org/10.25573/serc.11317820.

2.5. Data Analysis

Errors were calculated as either the standard deviation of the mean or by error propagation (e.g., Taylor, 1997). To make statistical comparisons, data were first tested for normality by the Kolmogorov-Smirnov test ($\alpha = 0.05$). Regression analysis was used when creating calibration curves to solve for ρ_{DB} and C_{org}. The Kruskal-Wallis H test ($\alpha = 0.05$) was used in comparisons between estuaries and wetland types because sample sizes are unequal. Because correlations were not assumed linear, Spearman's rank correlation test was used ($\alpha = 0.05$; Conover, 1980).

3. Results

3.1. Dry Bulk Density and Organic Carbon Calibrations

CT images showed that the cores were in good shape following extraction and transport, as biogenic and sedimentary structures typical of wetland sediment were well preserved within the top 50 cm of each core, and no obvious artifacts were present (Figure S1). Roots and rhizomes were abundant throughout the top 50 cm. When concentrated toward the surface, these dense root mats may prevent bioturbation (e.g., Kolker et al., 2009), explaining the lack of obvious burrows. Binned CT X-ray attenuation measured on an 8-bit grayscale (0–255) had a strong, positive relationship with ρ_{DB} ($\rho_{DB} = (0.069 \pm 0.003)\, e^{(0.023 \pm 0.001) \times CT}$, $R^2 = 0.98$, $n = 10$; Figure 2).

Mean bulk densities were observed to be significantly different between wetland types, with the lowest in high marsh and scrub-shrub cores, and the highest in the mudflat cores (Table 2; Kruskal-Wallis test, $p = 6 \times 10^{-8}$, $n = 3$). When plotted along a standardized elevation gradient, z^*, ρ_{DB} decreases with increased elevation (Figure 3a). Others have observed similar trends (e.g., Callaway et al., 2012; Roner et al., 2016; Thorne et al., 2014), whereby low tidal elevations are inundated longer resulting in greater deposition of lithogenic material (Mudd et al., 2009). When compared between high marshes, mean ρ_{DB} were significantly different between estuaries as well, the highest and lowest of which were in Coquille and Youngs, respectively (Kruskal-Wallis test, $p = 0.007$, $n = 7$).

There was a strong relationship ($C_{org} = (0.23 \pm 0.03)\, OM^2 + (0.28 \pm 0.01)\, OM$, $R^2 = 0.98$, $n = 66$) between LOI-derived OM and C_{org} measured by elemental analysis (Figure 4). The conversion factor of 0.28 ± 0.01 is similar to conversion factors calculated by others, such as 0.40 ± 0.01 by Craft et al. (1991) and 0.421 ± 0.012 by

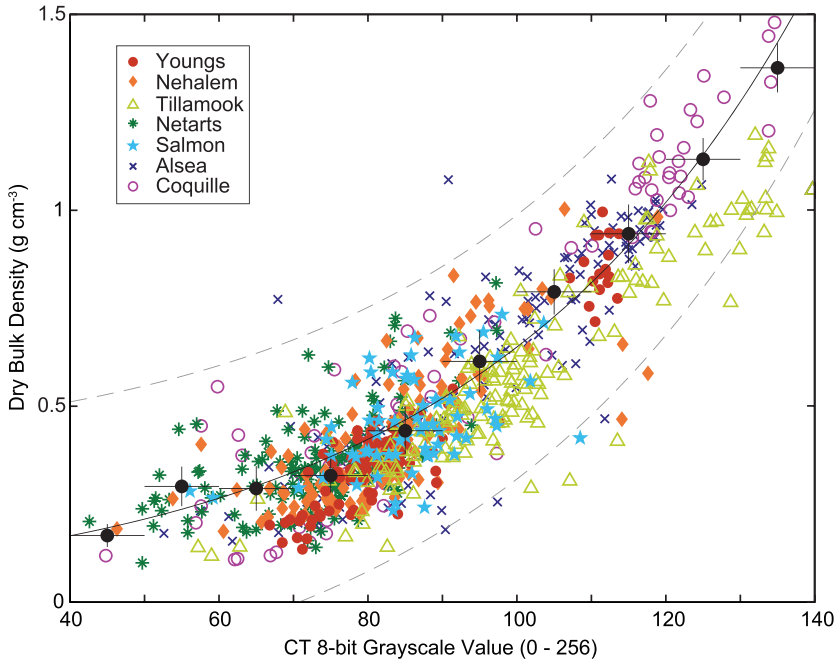

Figure 2. The relationship between dry bulk density (ρ_{DB}) measured gravimetrically within 2-cm increments with depth within numerous cores and CT-derived 8-bit grayscale value (0–255) measured in the corresponding depth increments. Data ($n = 829$) were binned into 10 grayscale units and displayed as black dots. The vertical and horizontal error bars on the binned data represent the standard deviations of the average ρ_{DB} and CT grayscale value in each bin, respectively. The regression equation (black line) was calculated using the binned data and is $\rho_{DB} = (0.069 \pm 0.003)\, e^{(0.023 \pm 0.001) \times CT}$ ($R^2 = 0.98$, $n = 10$). The gray dashed lines depict the 95% confidence bounds.

Holmquist et al. (2018b). Given the closeness of fit for all of the estuaries, 0.28 ± 0.01 is appropriate for least-disturbed wetland sediments in Oregon.

Comparison of mean C_{org} contents of each core revealed significantly higher values within high marsh and scrub-shrub sediments ($9.0 \pm 3.3\%$) and much lower values within mudflat cores ($2.0 \pm 0.8\%$; Kruskal-Wallis test, $p = 6 \times 10^{-9}$, $n = 3$). Despite interestuarine differences in ρ_{DB}, C_{org} contents were not significantly different between the high marshes of the different estuaries (Kruskal-Wallis test, $p = 0.07$, $n = 7$). When plotted along a standardized elevation gradient, z^*, C_{org} contents increased with increased elevation (Figure 3b). Others have observed similar trends (Chmura et al., 2001; Roner et al., 2016). Decreased tidal inundation at higher elevations decreases mineral input and also reduces inundation stress, which leads to increased productivity and higher amounts of autochthonous carbon (Friedrichs & Perry, 2001).

3.2. Sediment and Carbon Burial Rates

All cores either had no ^{137}Cs activities above the detection limit or exhibited anomalous ^{137}Cs profiles indicative of postdepositional remobilization (Foster et al., 2006), in which the activity peaked at or near the sediment surface and was much higher (40–320 Bq kg^{-1}) than expected given unaltered adsorption. Therefore, the ^{137}Cs data were not used in determining accumulation rates.

When determining excess ^{210}Pb-derived vertical accretion rates by the CIC method, data points were excluded from the regressions for the following reasons: errors below the detection limit of the γ-ray spectrometers (3 Bq kg^{-1}), surface sediment OM contents that diluted the lithogenic component causing low excess ^{210}Pb activities, or outliers due possibly to a change in lithology. Cores without excess ^{210}Pb, with excess ^{210}Pb profiles that were indicative of nonsteady state sediment accumulation, or with CT scans that revealed extensive bioturbation were not included in the analysis. Of the 72 cores collected, three quarters (54) had interpretable excess ^{210}Pb profiles: 4 scrub-shrub wetland (80%), 43 high marsh (96%), 6 low marsh (50%), and 1 mudflat (10%) cores. Because scrub-shrub wetlands are similar in elevation to high marsh, these will be considered together under the heading high marsh/scrub-shrub. Because fewer mudflat and low marsh

Journal of Geophysical Research: Biogeosciences

10.1029/2019JG005464

Table 2

Number of Sediment Cores (n; Values in Parentheses Indicate a Different Count for Cores That Returned Interpretable Excess ^{210}Pb Profiles) Collected Within Each Wetland Type Within the Seven Estuaries, and Sediment Properties Measured Include Relative Elevation (z; Values Are Means and Standard Deviations When n ≥ 2), Dry Bulk Density (ρ_{DB}), Organic Carbon (C_{org}) Content, and C_{org} Density*

		Youngs	Nehalem	Tillamook	Netarts	Salmon	Alsea	Coquille
Mudflat	*n*	0	2 (0)	0	3 (1)	0	3 (0)	2 (0)
	*z**		−0.15 ± 0.10		0.50 ± 0.12		0.23 ± 0.14	0.32 ± 0.01
	ρ_{DB} (g cm^{-3})		0.94 ± 0.22		0.76 ± 0.11		0.80 ± 0.13	1.2 ± 0.1
	C_{org} (%)		2.6 ± 1.1		2.1 ± 0.5		2.7 ± 0.7	0.86 ± 0.00
	C_{org} density (g C_{org} cm^{-3})		0.022 ± 0.004		0.015 ± 0.003		0.020 ± 0.002	0.010 ± 0.000
	SAR (mm yr^{-1})				2.3 ± 0.4			
	MAR (kg m^{-2} yr^{-1})				1.3 ± 0.2			
	CAR (g C_{org} m^{-2} yr^{-1})				51 ± 8			
Low marsh	*n*	1	3 (1)	2 (0)	0	0	3	3 (1)
	*z**	0.31	0.36 ± 0.19	0.59 ± 0.11			0.86 ± 0.13	0.55 ± 0.10
	ρ_{DB} (g cm^{-3})	0.74 ± 0.16	0.76 ± 0.10	0.72 ± 0.07			0.48 ± 0.03	1.1 ± 0.1
	C_{org} (%)	3.1 ± 1.2	2.8 ± 0.5	4.4 ± 0.6			7.2 ± 1.0	1.8 ± 0.7
	C_{org} density (g C_{org} cm^{-3})	0.022 ± 0.004	0.019 ± 0.002	0.030 ± 0.001			0.032 ± 0.004	0.014 ± 0.003
	SAR (mm yr^{-1})	2.0 ± 0.3	2.8 ± 0.4				2.0 ± 0.2	1.9 ± 0.5
	MAR (kg m^{-2} yr^{-1})	1.1 ± 0.1	1.3 ± 0.2				0.80 ± 0.10	1.1 ± 0.1
	CAR (g C_{org} m^{-2} yr^{-1})	54 ± 8	49 ± 7				67 ± 21	50 ± 13
High marsh/scrub-shrub	*n*	4	7 (5)	4	15 (14)	8 (7)[a]	7	5
	*z**	1.04 ± 0.10	0.87 ± 0.16	1.02 ± 0.16	1.71 ± 0.11	1.30 ± 0.07	1.15 ± 0.08	1.12 ± 0.12
	ρ_{DB} (g cm^{-3})	0.41 ± 0.03	0.46 ± 0.04	0.52 ± 0.09	0.42 ± 0.10	0.43 ± 0.08	0.49 ± 0.10	0.70 ± 0.12
	C_{org} (%)	4.2 ± 2.2	7.6 ± 1.3	9.2 ± 5.3	9.4 ± 3.1	11 ± 4	8.1 ± 1.6	5.7 ± 2.5
	C_{org} density (g C_{org} cm^{-3})	0.012 ± 0.007	0.032 ± 0.003	0.042 ± 0.013	0.035 ± 0.009	0.045 ± 0.007	0.037 ± 0.007	0.025 ± 0.006
	SAR (mm yr^{-1})	2.5 ± 0.7	2.9 ± 1.0	2.0 ± 0.2	1.9 ± 0.6	1.6 ± 0.3	1.7 ± 0.4	1.3 ± 0.3
	MAR (kg m^{-2} yr^{-1})	0.97 ± 0.31	1.1 ± 0.5	1.0 ± 0.2	0.72 ± 0.28	0.58 ± 0.11	0.69 ± 0.16	0.64 ± 0.36
	CAR (g C_{org} m^{-2} yr^{-1})	107 ± 43	120 ± 39	88 ± 20	74 ± 41	79 ± 21	63 ± 19	52 ± 7

Note. Accumulation rates include sediment (SAR), mass (MAR), and C_{org} (CAR).
[a]One Salmon River core returned a statistically different SAR and was therefore not included in mean calculations for the estuary.

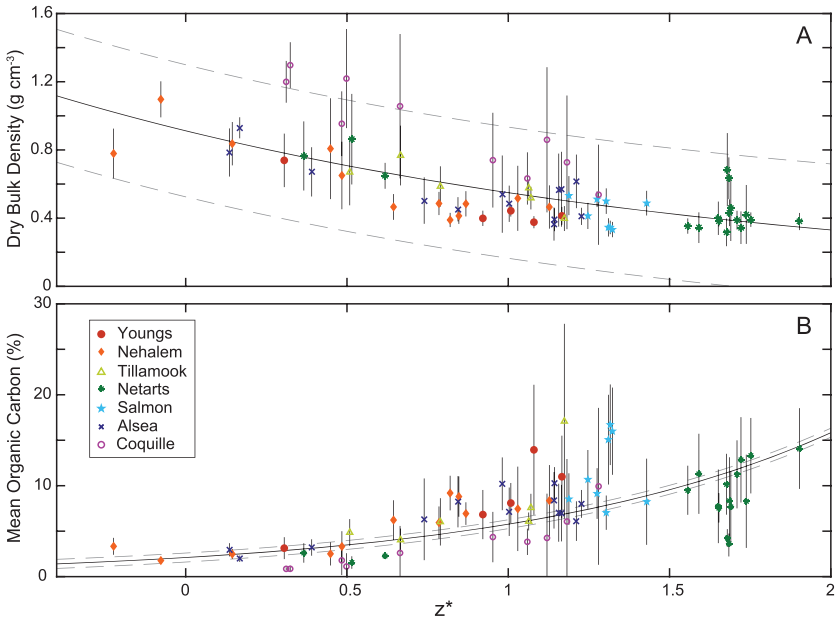

Figure 3. Relationship between (a) mean dry bulk density (ρ_{DB}) and (b) mean organic carbon (C_{org}) estimated every 2 cm within the top 50 cm and standardized elevation (z^*) of each core. Error bars indicate the standard deviations of the means. The solid black lines plot the correlation between ρ_{DB} and z^* and C_{org} and z^*; the gray dashed lines depict the 95% confidence bounds.

cores were collected and so few of those collected returned readily interpretable excess ^{210}Pb profiles, analyses associated with accumulation rates and carbon burial will predominately focus on high marsh/scrub-shrub cores.

Accretion rates ranged from 0.8 ± 0.2 to 4.1 ± 0.2 mm yr^{-1} among all high marsh/scrub-shrub cores, and standard errors ranged from ±0.1 to 0.5 mm yr^{-1}. These rates are comparable to others measured in tidal saline wetlands (Crosby et al., 2016; Kirwan, Temmerman, et al., 2016). The SAR ranges within the high marshes/scrub-shrubs of individual estuaries were as follows: 2.0 ± 0.2 to 3.4 ± 0.1 mm yr^{-1} in Youngs, 1.7 ± 0.2 to 4.1 ± 0.2 mm yr^{-1} in Nehalem, 1.7 ± 1.1 to 2.2 ± 0.3 mm yr^{-1} in Tillamook, 0.8 ± 0.2 to 3.0 ± 0.1 mm yr^{-1} in Netarts, 1.2 ± 0.2 to 2.9 ± 0.3 mm yr^{-1} in Salmon, 1.2 ± 0.2 to 2.1 ± 0.1 mm yr^{-1} in Alsea, and 1.1 ± 0.2 to 1.8 ± 0.1 mm yr^{-1} in Coquille.

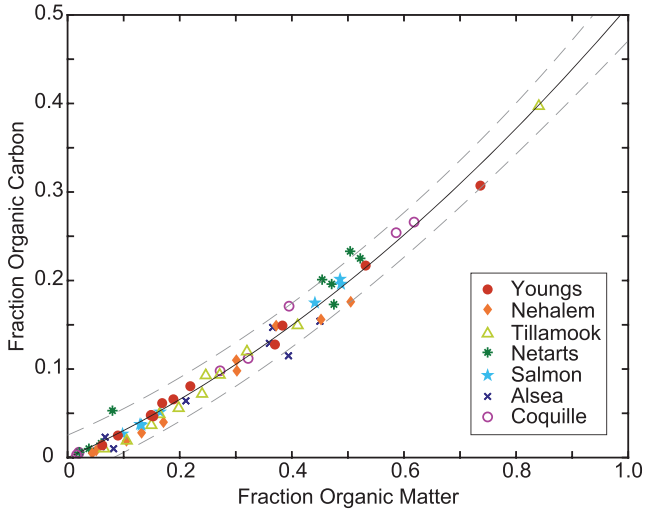

Figure 4. The relationship between fraction organic matter (OM) as determined by loss on ignition (LOI) and organic carbon (C_{org}) measured by elemental analysis in a subset of samples from the seven estuaries (n = 66). The regression equation (black line) is C_{org} = (0.23 ± 0.03) OM^2+(0.28 ± 0.01) OM (R^2 = 0.98). The gray dashed lines depict the 95% confidence bounds. The subset was selected to include a range in OM contents from at least four cores from each estuary to ensure a representative curve.

C_{org} burial rates ranged from 19 ± 4 to 160 ± 20 g C_{org} m^{-2} yr^{-1} among all high marsh/scrub-shrub cores. These rates are comparable to others measured in tidal saline wetlands (Ouyang & Lee, 2014). The CAR ranges within the high marshes/scrub-shrubs of individual estuaries were as follows: 58 ± 7 to 160 ± 10 g C_{org} m^{-2} yr^{-1} in Youngs, 59 ± 6 to 150 ± 10 g C_{org} m^{-2} yr^{-1} in Nehalem, 69 ± 8 to 120 ± 10 g C_{org} m^{-2} yr^{-1} in Tillamook, 19 ± 4 to 160 ± 20 g C_{org} m^{-2} yr^{-1} in Netarts, 45 ± 8 to 130 ± 20 g C_{org} m^{-2} yr^{-1} in Salmon, 42 ± 8 to 94 ± 9 g C_{org} m^{-2} yr^{-1} in Alsea, and 43 ± 11 to 60 ± 4 g C_{org} m^{-2} yr^{-1} in Coquille.

Mean carbon contents and CARs measured within cores collected from scrub-shrub wetlands from Youngs (n = 2), Tillamook (n = 1), and Netarts (n = 2; only 1 core provided accumulation rate data) were comparatively high. Mean C_{org} contents within the top 50 cm of scrub-shrub wetland cores averaged 13.0 ± 3.4% (n = 5) compared to an average of 8.5 ± 3.0% (n = 45) for high marsh cores. The

mean CAR within scrub-shrub wetlands, 120 ± 30 g C_{org} m^{-2} yr^{-1} (n = 4), additionally exceeded the mean CAR of 77 ± 35 g C_{org} m^{-2} yr^{-1} (n = 43) measured within high marshes.

4. Discussion

4.1. Data Assessment

Before discussing the observed patterns, we examine the quality of the measurements. The majority of scrub-shrub wetland and high marsh and some low marsh cores displayed excess ^{210}Pb downcore profiles that approximated idealized profiles (MacKenzie et al., 2011) and were therefore readily interpretable (Figure S2). Based on the lack of bioturbation evidence within the CT scans, we concluded that none of the high marsh/scrub-shrub cores were subject to substantial bioturbation. It is likely that the presence of dense root mats common to tidal wetlands may have prevented much mixing.

To investigate whether the sediment core locations were net depositional or erosional, inventories of excess ^{210}Pb (Bq cm^{-2}) were calculated using standard techniques (Cochran et al., 1998). These inventories were compared to an estimate of annual atmospheric flux of ^{210}Pb, assumed constant by the CIC model. However, the atmospheric flux of ^{210}Pb is spatially variable (Baskaran, 2011), and few values are published for the PNW. Nevissi (1985) measured 0.0073 ± 0.004 Bq cm^{-2} yr^{-1} in Seattle (WA); Balistrieri et al. (1995) and Barnes et al. (1979) have published similar values measured at nearby Lake Sammamish (WA) and Lake Washington (WA), respectively. Atmospheric ^{210}Pb flux is correlated to latitude, and this value corresponds well with other measured fluxes within 40–50°N (0.0155 ± 0.0075 Bq cm^{-2} yr^{-1}; Baskaran, 2011). Since the Oregon coast falls within this latitude range, we can assume that the steady state inventory of atmospheric ^{210}Pb is 0.24 ± 0.13 Bq cm^{-2}.

The mean excess ^{210}Pb inventory for all sediment cores was 0.53 ± 0.29 Bq cm^{-2}. These locations were therefore net depositional. Although the average was similar to the expected excess ^{210}Pb inventories if the radionuclide was primarily supplied by atmospheric flux, fluvially supplied excess ^{210}Pb appeared to contribute additionally to the inventories. The mean excess ^{210}Pb inventory varied significantly between estuaries (Kruskal-Wallis test, $p = 5 \times 10^{-4}$, n = 7) with the greatest mean value in Netarts (0.69 ± 0.35 Bq cm^{-2}) and the lowest in the Coquille (0.29 ± 0.19 Bq cm^{-2}). The mean excess ^{210}Pb inventory also varied significantly between wetland types (Kruskal-Wallis test, $p = 3 \times 10^{-5}$, n = 3), with the highest values in scrub-shrub wetland and high marsh, and the lowest values in low marsh and mudflat.

Our results are comparable to previously measured rates of accretion along the Oregon coast. Accretion rates, measured using ^{137}Cs, at tidal marsh sites in Siletz Bay, Coos Bay, and Coquille River Estuary (also known as Bandon Marsh) averaged 3.3 ± 1.2 (n = 3), 3.3 ± 0.1 (n = 3), and 2.3 ± 0.2 (n = 3) mm yr^{-1}, respectively (Thorne et al., 2018). The range of high marsh SARs in the Coquille was lower in our study (1.1 ± 0.2 to 1.8 ± 0.1 mm yr^{-1}), possibly a result in differences between radiometric methods, especially challenges of the ^{137}Cs methods applied to Pacific NW estuaries (Drexler et al., 2018). The range of SARs measured in the Salmon River Estuary (1.2 ± 0.2 to 2.9 ± 0.3 mm yr^{-1}) was lower than a previously measured rate of 3.0 ± 0.0 mm yr^{-1} (n = 2) by Thom (1992) along the northern edge of the estuary. The difference in SARs may be because Thom's (1992) preliminary study obtained only two ^{137}Cs-derived vertical accretion rates that were likely influenced by nearby dikes. Although dikes usually prevent inundation, thus slowing accretion and causing elevation loss through OM oxidation, dikes may also alter local hydrodynamics, resulting in increased sediment accumulation in nearby, unrestricted areas (Hood, 2004). It is also possible that in the time between Thom's (1992) collection and this study's core collection, accretion rates may have slowed within the least-disturbed portions of the Salmon River Estuary.

In determining mean SARs representative of each estuary's tidal saline wetlands, heterogeneity within the environment necessitates comprehensive sampling (Fourqurean et al., 2014). Between 4 to 14 cores returned interpretable ^{210}Pb profiles from the high marshes/scrub-shrubs of each estuary. Even in the estuaries with only four SARs, there was good agreement in accretion rates. In fact, there were no outliers of accretion rates within each estuary except in the Salmon River Estuary (SR01; Grubb's test, $\alpha = 0.05$), and this value was excluded from mean rate calculations. Less heterogeneity within each estuary was therefore present than expected. More studies are needed to assess the impact of sampling scheme (e.g., number of cores, transect versus random sampling) on accuracy when determining mean SARs for the high marsh and an entire

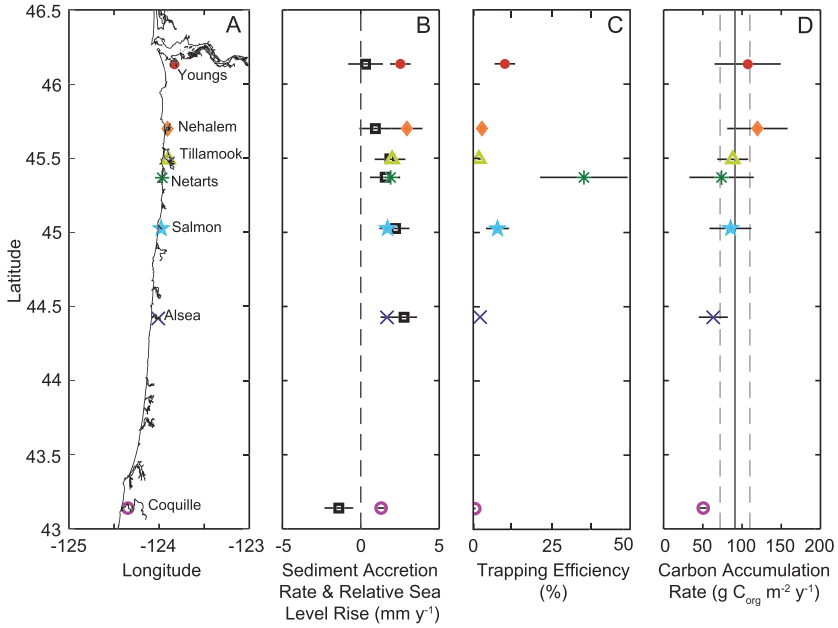

Figure 5. (a) Location of each estuary along the Oregon coast. (b) Comparison of mean high marsh/scrub-shrub sediment accretion rate (SAR) depicted as a colored shape and relative sea level rise (RSLR) depicted as an open square for each estuary. The sediment accretion error bars represent the standard deviation of the mean and the RSLR error bars represent propagated error. The dashed line indicates 0-mm yr^{-1} RSLR. (c) Trapping efficiency for each estuary calculated using mean mass accumulation rates, tidal wetland areas, and estimated sediment loads. The error bars represent standard propagation of error using the standard deviation of the mean mass accumulation rate. (d) Mean high marsh/scrub-shrub carbon accumulation rates (CAR). The error bars represent the standard deviation of the mean. The solid line and gray dashed lines indicate the global mean and standard deviation 91 ± 19 g C_{org} m^{-2} yr^{-1} (IPCC, 2013).

estuary, as others have done for assessing the heterogeneity of salt marsh carbon stocks (van Ardenne et al., 2018).

High marsh/scrub-shrub SARs were statistically different between estuaries (Kruskal-Wallis test, $p = 0.01$, $n = 7$). Mean accretion rates for the high marsh/scrub-shrub sites in Oregon ranged from 1.3 ± 0.3 mm yr^{-1} in Coquille River estuary to 2.9 ± 1.0 mm yr^{-1} in Nehalem Bay (Table 2). It is therefore apparent that differences in mean SARs among Oregon estuaries result from estuary-specific variations in accretion rate drivers.

4.2. Oregon Tidal Saline Wetland Resistance to Drowning

Assessment of marsh vulnerability to drowning typically involves comparison of vertical accretion to the rate of RSLR (e.g., Cahoon et al., 1996; FitzGerald et al., 2008; Reed, 1995). Along the Oregon coast, the northernmost and southernmost high marshes/scrub-shrubs have kept pace with RSLR over the last century (Figure 5b) and in some cases (i.e., Youngs, Nehalem, and Coquille), the mean high marsh/scrub-shrub SAR exceeds RSLR.

Interestingly, although relative sea level is actually falling within the Coquille River Estuary due to rapid interseismic uplift (Burgette et al., 2009), SARs were positive in this area. Typically, under scenarios of negative accommodation space (i.e., regressions) coastal areas are expected to experience erosion. Although the excess ^{210}Pb inventory for this estuary was the lowest among the seven estuaries, it did not appear to be erosive given that the mean value fell well within the expected range of inventories for steady state atmospheric input of ^{210}Pb. As mentioned previously, Thorne et al. (2018) actually measured a higher mean SAR for the Coquille. Furthermore, others have observed horizontal expansion of the tidal marsh in the lower Coquille River Estuary during the past 150 years (Benner, 1992; Dicken et al., 1961). We therefore conclude that accretion in the Coquille River Estuary has greatly exceeded expected accumulation rates under falling sea level (i.e., erosion). Possible explanations for the observed excess accumulation rates in Youngs, Nehalem, and Coquille will be explored in the next section.

Along the central coast, lower mean SARs than estimated RSLR rates in Salmon and Alsea high marshes indicated possible drowning or a lag in vertical growth. Although the difference in mean rates was not statistically significant, the reason for this apparent instability could be that these estuaries are located along the section of the Oregon coast that experiences the highest rates of RSLR. However, even 2.8 ± 0.8-mm yr^{-1} RSLR is not greatly higher than rates observed elsewhere where salt marshes are accreting at a pace similar to or greater than RSLR (e.g., Kolker et al., 2009). Moreover, models predict that salt marshes are capable of SARs up to 50 mm yr^{-1} (Kirwan, Temmerman, et al., 2016).

Conversely, limited suspended sediment may inhibit accretion. Indeed, low suspended sediment concentrations are responsible for most cases of marsh drowning (e.g., Mississippi River Delta, Chesapeake Bay, and Venice Lagoon; Weston, 2014) and models (e.g., Kirwan et al., 2010) have concluded that sediment availability strongly determines the maximum rate of sea level rise with which salt marshes may keep pace. However, suspended sediment does not appear limited within these systems.

Rough estimates of the trapping efficiency of each wetland, calculated by comparing the total annual mass accumulation rates (mean high marsh/scrub-shrub Mass accumulation rate multiplied by tidal wetland area) with mean annual fluvial sediment load, revealed no dearth of suspended sediment in these systems (Figure 5c). Tidal saline wetlands in Salmon and Alsea have trapped approximately 8 and 2% of available suspended sediment, respectively. Comparison to Netarts Bay is particularly revealing. Despite receiving only 2.5×10^3 t yr^{-1} of fluvial suspended sediment and experiencing moderately fast RSLR (1.5 ± 1.0 mm yr^{-1}), Netarts tidal saline wetlands have a trapping efficiency of ~35% and appear to have kept pace with rising sea level. Thus, even considering uncertainty in estimating sediment-trapping efficiency, it does not seem likely that Oregon estuaries, including Salmon or Alsea, are sediment-limited systems. Future studies should examine other indicators of marsh drowning, including ponding, channel expansion, and horizontal retreat (e.g., DeLaune et al., 1994; Mariotti & Fagherazzi, 2013; Watson et al., 2017) to confirm these results.

Our results shed light on tidal saline wetland resilience to drowning in the face of twentieth-century RSLR. Projecting these results forward in time is complex. On one hand, salt marshes along the northern and southern Oregon coast appear resistant to drowning. RSLR rates in these areas are slow or even falling, high marsh/scrub-shrub SARs have kept pace with RSLR, and suspended sediment supply does not appear to be a limiting factor. Vertical accretion rates at lower elevations are an additional indication of tidal wetland resilience under future rates of RSLR (Kirwan, Temmerman, et al., 2016). High marsh/scrub-shrub vertically accretes to a high elevation within the tidal frame, thereby reducing frequent flooding, but low marsh is often inundated, simulating the stress of accelerated RSLR. Because low marsh accretion rates within Youngs (2.0 ± 0.3 mm yr^{-1}, $n = 1$), Nehalem (2.8 ± 0.4 mm yr^{-1}, $n = 1$), and Coquille (1.9 ± 0.5 mm yr^{-1}, $n = 1$; Table 2) have kept pace with RSLR, these areas may continue accreting under such stress, avoiding future drowning.

Yet the relatively low accretion rates within the two estuaries experiencing the fastest rates of RSLR, despite no clear sediment limitation, is troublesome. Low marsh SARs within Alsea (2.0 ± 0.2 mm yr^{-1}, $n = 3$; Table 2), though higher than high marsh SARs, were lower than RSLR, as well. Results of Thorne et al. (2018) additionally predict widespread loss of high marsh by the end of the century along the Oregon coast under high sea level rise scenarios. Future studies should focus on confirming these results and determining causes of observed drowning in Salmon and Alsea.

4.3. Drivers of Sediment Accretion

Models of salt marsh growth often assume a relationship between elevation and sediment accretion rate (e.g., Fagherazzi et al., 2012; French, 2006; Morris et al., 2002; Swanson et al., 2014) based on empirical evidence (e.g., Cahoon & Reed, 1995; Stoddart et al., 1989; Temmerman et al., 2003). These relationships depict decreasing sediment accumulation rate with increased elevation due to decreased hydroperiod higher in the tidal frame. Moreover, high accretion rates related to in situ OM contribution may be expected at elevations at which plant productivity peaks. Plant dry mass measured by "marsh organ" experiments of *Juncus balticus*, present in a number of Oregon high marshes (i.e., Nehalem, Netarts, Salmon, Alsea, and Coquille), declines monotonically with increased inundation (Janousek et al., 2016).

Despite these possible relationships between accretion and elevation, comparison of high marsh/scrub-shrub SARs as a function of z^* for Oregon estuaries produced no distinct relationship (Figure 6a);

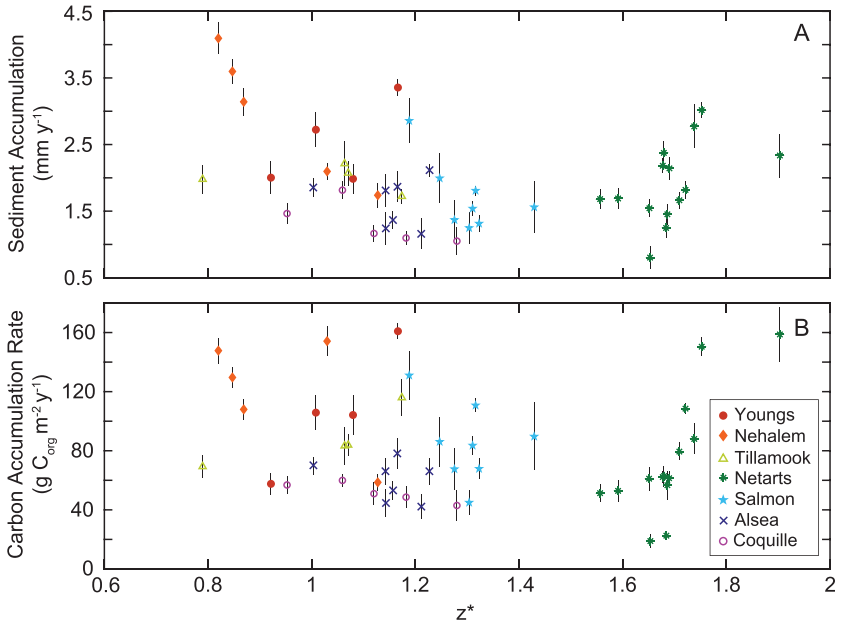

Figure 6. Lack of relationship between relative elevation (z^*) and (a) sediment accumulation rate (SAR) and (b) organic carbon burial rate (CAR) measured within high marsh-scrub shrub sediment cores from different Oregon estuaries. Error bars indicate the error of the rate estimate.

correlation between these two variables revealed no dependence (Spearman's rank correlation, $\rho = -0.2$, $n = 47$). Within each estuary, local variations in vegetation assemblage, above-ground and below-ground C_{org} production, allochthonous C_{org} accumulation, channel density, and surface flow velocities may obscure any obvious elevation trends. Additionally, a wider range of elevations may be necessary to produce a clear relationship. Acquiring additional SAR data at low elevations may be challenging given the low percentage (10% and 50%) of interpretable excess ^{210}Pb profiles for mudflats and low marshes, respectively.

Our results call for a reassessment of the approach and results of Thorne et al. (2018), who predict extensive conversion of U.S. West Coast tidal wetlands to unvegetated habitat by the end of the twenty-first century under high sea level rise scenarios. At a minimum, the lack of a clear relationship between SAR and elevation in our data suggests that determining such a relationship requires numerous, well-distributed measurements. To parameterize their model, Wetland Accretion Rate Model of Ecosystem Resilience (Swanson et al., 2014), Thorne et al. (2018) used empirical relationships of mineral and carbon accumulation rates as a function of elevation relative to mean tide level. The empirical relationships were based on work conducted in San Francisco Bay by Swanson et al. (2014) and were calibrated within each estuary based on measured accumulation rates. However, Thorne et al. (2018) calibrated the empirical relationships using only three ^{137}Cs-derived accretion rates within each of the three Oregon estuaries—Siletz, Coos, and Coquille. The elevations of these cores varied by only 0.5 to 1.4 m. Given that the Wetland Accretion Rate Model of Ecosystem Resilience model employed by Thorne et al. (2018) predicts elevation changes in relation to sea level by incorporating mineral sediment accumulation rates at different elevations, this relationship should be region-specific and calibration data must span a greater elevation range.

Given that mean SARs were higher than RSLR within Youngs, Nehalem, and Coquille, it appears that tidal saline wetland accretion must be controlled by a variable other than elevation. Logically, we turn to suspended sediment load.

A comparison of accretionary balance (the difference between SAR and RSLR; Callaway et al., 1996) and relative sediment load would presumably produce a positive relationship in which excess accretion could be explained by high sediment supply. Alsea and Salmon were excluded from this analysis as both high marshes had negative accretionary balances, and thus appear to be drowning. Youngs River Estuary was also not included in the correlation. Youngs River Estuary, which has an approximately stable RSLR (0.3 ± 1.1 mm yr^{-1}), has accreted at a mean rate of 2.5 ± 0.7 mm yr^{-1} within the high marsh/scrub-shrub, which is

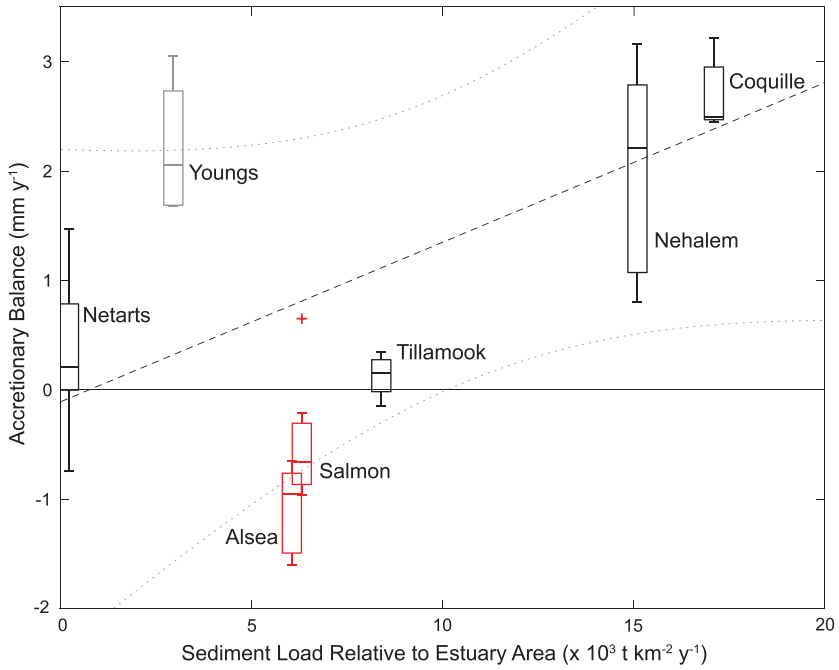

Figure 7. The relationship between the accretionary balance, which is the high marsh/scrub-shrub sediment accretion rate minus relative sea level rise (RSLR), and the sediment load (estimated by the USGS SPARROW model; Wise, 2018) relative to estuary area. Within each box, the central mark indicates the median, while the top and bottom of the box indicate the 25th and 75th percentiles, respectively. The whiskers on each box indicate the spread of the data excluding outliers. The "cross" symbol represents an outlier (SR01). The black, dashed line depicts the correlation between accretionary balance and relative sediment load, and the gray dashed lines depict the 95% confidence bounds. Youngs River Estuary, colored gray, and Alsea Bay and Salmon River Estuary, colored red, were not included in the correlation.

8 times faster than the estimated RSLR. Inherent in our comparison of accretionary balance to fluvial sediment load relative to estuary area was the assumption that no additional sediment is supplied through inlets or resuspended from within the estuaries. This assumption was particularly unlikely within Youngs as the bay shares an inlet with the Columbia River Estuary, with a load of roughly 10 Mt yr^{-1} (Milliman & Syvitski, 1992). Considering the apparent underestimation of suspended sediment load within Youngs River Estuary, the sediment trapping efficiency (10%) was likely overestimated.

Correlation between Nehalem, Tillamook, Netarts, and Coquille revealed that, indeed, there exists a strong, positive relationship between excess accretion and relative sediment load (Spearman's rank correlation, $\rho = 0.7$, $n = 28$; Figure 7). Our results add additional weight to previous findings that suspended sediment supply imposes a control on SAR (e.g., Colman & Bratton, 2003; Day et al., 2000; Gunnell et al., 2013; Kirwan et al., 2011). Furthermore, our results suggest that other regions with positive accretionary balances such as those observed in the compilations of Kirwan, Temmerman, et al. (2016) and Crosby et al. (2016) may be related to high suspended sediment supply, and future studies should seek to test this hypothesis.

Models of marsh platform accretion typically calculate additions to sediment volume as the sum of OM and mineral contributions (e.g., Allen, 2000; Fagherazzi et al., 2006; Fagherazzi et al., 2012; Kirwan et al., 2010; Kirwan, Walters, et al., 2016; Mariotti & Fagherazzi, 2010; Schile et al., 2014), the latter of which is determined by the depth-averaged suspended sediment concentration and the settling velocity integrated over the duration of flooding. These models tend to predict that under increased rates of RSLR, and thus increased duration of flooding, sediment accretion, especially facilitated through mineral deposition, will increase given no dearth of suspended sediment. What then, would we predict in instances in which relative sea level is neutral or falling? Based on these models, it logically follows that no accretion would occur. Despite this hypothesis, high marshes/scrub-shrubs in both Youngs and Coquille, which experience RSLR rates of 0.3 ± 1.1 and -1.4 ± 0.9 mm yr^{-1}, respectively, are accreting apparently as a result of high annual average suspended sediment loads relative to estuary area. One possible explanation for continued

sediment accumulation under these RSLR conditions, which requires further investigation along the Oregon coast, is that storms and other episodic, high-water events (e.g., exceptionally high tides) may play an important role in controlling long-term accretion, as others have observed (e.g., Cahoon, 2006; Castagno et al., 2018; Goodbred & Hine, 1995; Reed, 1989; Turner et al., 2006; Tweel & Turner, 2014) and as some are incorporating into morphodynamic models (Schuerch et al., 2013). Models of tidal wetland morphodynamics thus require better integration with data collected from field observations and experiments, especially in locations that have high capacity to expand our limits of understanding (Wiberg et al., 2020), such as those that exhibit relative sea level fall and highly episodic sediment fluxes.

4.4. Blue Carbon Burial Rates

Although the importance of C_{org} burial in tidal saline wetlands within global carbon budgets is widely recognized, many coasts, including that of Oregon, lack published data. To our knowledge, our results are the first published rates of carbon burial within Oregon. Moreover, we provide data for the comparatively understudied tidal saline wetland type—scrub-shrub wetlands.

Mean sediment carbon density in vegetated sites averaged 0.034 ± 0.011 g C_{org} cm^{-3}, similar to both the conterminous U.S. mean of 0.027 ± 0.013 g C_{org} cm^{-3} (Holmquist et al., 2018a) and the global mean of 0.039 ± 0.003 g C_{org} cm^{-3} for tidal wetlands (Chmura et al., 2003). The mean carbon burial rate within the high marshes/scrub-shrubs of all estuaries, 81 ± 36 g C_{org} m^{-2} yr^{-1}, was additionally comparable to the global burial flux of 91 ± 19 g C_{org} m^{-2} yr^{-1} (IPCC, 2013; Figure 5d). Previous compilations of global tidal saline wetland carbon burial rates have used California data as representative of the entire U.S. West Coast (e.g., Chmura et al., 2003; Ouyang & Lee, 2014). However, Oregon tidal saline wetlands have accumulated carbon at roughly half the rate of 174 ± 45 g C_{org} m^{-2} yr^{-1} extrapolated for the Pacific Northwest based on California data (Ouyang & Lee, 2014). This discrepancy could be a result of relatively slower RSLR rates in Oregon estuaries, disagreement in classification of wetland types resulting in dissimilarity in tidal elevation of sampled wetlands, differences in the degree of disturbance, or latitudinal variation in temperature and productivity (Ouyang & Lee, 2014). As many others have suggested (e.g., Chmura, 2013; Mcleod et al., 2011), full knowledge of the role of coastal vegetated habitats in the global carbon cycle requires more measurements of blue carbon burial globally. Future assessments should include more measurement within scrub-shrub wetlands, especially considering the comparatively high rate of carbon burial (120 ± 30 g C_{org} m^{-2} yr^{-1}) within this wetland type.

Disentangling the relative drivers of tidal saline wetland CARs is challenging given the complexity of these systems. Accumulated organic matter may either be allochthonous, sourced from tidal or storm deposits as the organic fraction of accumulating sediment, or autochthonous, produced in situ by above- and belowground plant productivity. Net accumulation is also impacted by removal through erosion and decomposition. Because CARs are calculated as products of sediment C_{org} density and SAR, we look to these variables first.

SARs were strongly, positively correlated with rates of carbon burial ($R^2 = 0.49$), and others have found a similar relationship (e.g., Callaway et al., 2012; Chmura et al., 2003; Morris et al., 2016). But because this relationship is simply a correlation, the dependence between CAR and SAR may alternatively be interpreted as CARs drive SARs, especially since increasing OM deposition must necessarily increase sediment volume (Morris et al., 2016). However, CARs were less-well correlated with mean surface values of carbon density ($R^2 = 0.33$), indicating that factors driving SARs may be primarily influencing CARs in Oregon estuaries. Indeed, comparison of CARs as a function of z^* for Oregon estuaries produced no distinct relationship (Figure 6b), and correlation between these two variables revealed no apparent dependence (Spearman's rank correlation, $\rho = -0.1$, $n = 7$). Since both ρ_{DB} and C_{org} content showed a clear elevational influence (Figure 3), local variations in ecogeomorphic processes that impact SAR must have obscured any obvious elevation trends in CARs. Moreover, mean surface C_{org} contents were not statistically distinct between estuaries (Kruskal-Wallis test, $p = 0.07$, $n = 7$) while both CARs and SARs were significantly different between estuaries (Kruskal-Wallis test, $p = 0.02$, $n = 7$ and $p = 0.01$, $n = 7$, respectively). Thus, within Oregon estuaries, SAR and the factors influencing SAR—RSLR and relative sediment load—primarily controlled CAR. Because accretion rates appeared partially controlled by RSLR, as relative sea level rises and Oregon tidal

saline wetlands respond with increasing SARs, CARs may additionally rise so long as suspended sediment remains available.

5. Conclusions

We utilized the Oregon coast as a natural laboratory, measuring sediment accumulation and blue carbon burial rates over the last century within a range of tidal saline wetland types of seven estuaries that vary in both RSLR and relative sediment load. Firstly, our measurements greatly improve our understanding of both accretion rates (0.8 ± 0.2 to 4.1 ± 0.2 mm yr^{-1}) and blue carbon burial rates (19 ± 4 to 160 ± 20 g C_{org} m^{-2} yr^{-1}) along the Oregon coast, providing much needed data to regional researchers, land managers, and policy makers. Results indicated that most Oregon marshes have maintained a positive accretionary balance, with the exception of those in the central coast, which may be a result of comparatively high rates of RSLR. Also, our data supplement global assessments of tidal saline wetlands as we measured accumulation rates under relatively low RSLR rates (-1.4 ± 0.9 to 2.8 ± 0.8 mm yr^{-1}) and high relative sediment loads (0.23 to 17×10^3 t km^{-2} yr^{-1}). We additionally empirically demonstrated that sediment accumulation rates do not appear driven by elevation in Oregon tidal saline wetlands, but rather in instances in which marshes are not drowning, vertical accretion appears to be linked to both RSLR and suspended sediment supply. Lastly, blue carbon burial in Oregon is primarily controlled by sediment accretion rate, and thus, as sea level rise accelerates, carbon accumulation will increase so long as tidal saline wetlands maintain positive accretionary balances.

Acknowledgments
Digital data can be accessed through the Smithsonian Environmental Research Center's Coastal Carbon Research Coordination Network (doi.org/10.25573/serc.11317820). Archived halves of each sediment core are stored at the Oregon State University Marine and Geology Repository (http://osu-mgr.org). This study was funded by Oregon Sea Grant, Bonneville Power Administration, U.S. Fish and Wildlife Service, National Oceanic and Atmospheric Administration, and Oregon Watershed Enhancement Board. We thank G. Molino, I. Garris, and J. Turner for the sample preparation, Miguel Goñi for his help with carbon analysis, Dan Wise (USGS) with his help estimating suspended sediment load, and our field volunteers (L. Brown, M. Ewald, N. Elasmar, S. Mahaffey, M. Sepp, J. Siemens, J. Spruel, J. Turner, and the 2010–2018 Cascadia crews, and others). Additionally, we appreciate the thoughtful comments of the editors and the mail reviewers.

References

Allen, J. R. (2000). Morphodynamics of Holocene salt marshes: A review sketch from the Atlantic and Southern North Sea coasts of Europe. *Quaternary Science Reviews*, *19*(12), 1155–1231. https://doi.org/10.1016/S0277-3791(99)00034-7

Arias-Ortiz, A., Masqué, P., Garcia-Orellana, J., Serrano, O., Mazarrasa, I., Marbà, N., et al. (2018). Reviews and syntheses: ^{210}Pb-derived sediment and carbon accumulation rates in vegetated coastal ecosystems—Setting the record straight. *Biogeoscineces*, *15*(22), 6791–6818. https://doi.org/10.5194/bg-15-6791-2018

Balistrieri, L. S., Murray, J. W., & Paul, B. (1995). The geochemical cycling of stable Pb, ^{210}Pb, and ^{210}Po in seasonally anoxic Lake Sammamish, Washington, USA. *Geochimica et Cosmochimica Acta*, *59*(23), 4845–4861. https://doi.org/10.1016/0016-7037(95)00334-7

Barbier, E. B., Hacker, S. D., Kennedy, C., Koch, E. W., Stier, A. C., & Silliman, B. R. (2011). The value of estuarine and coastal ecosystem services. *Ecological Monographs*, *81*(2), 169–193. https://doi.org/10.1890/10-1510.1

Barnes, R. S., Birch, P. B., Spyridakis, D. E., & Schell, W. R. (1979). Changes in the sedimentation histories of lakes using lead-210 as a tracer of sinking particulate matter. In *Isotope hydrology* (Vol. 2, pp. 875–897). Vienna, Austria: International Atomic Energy Agency (IAEA).

Baskaran, M. (2011). Po-210 and Pb-210 as atmospheric tracers and global atmospheric Pb-210 fallout: A review. *Journal of Environmental Radioactivity*, *102*(5), 500–513. https://doi.org/10.1016/j.jenvrad.2010.10.007

Beck, M. W., Heck, K. L., Able, K. W., Childers, D. L., Eggleston, D. B., Gillanders, B. M., et al. (2001). The identification, conservation, and management of estuarine and marine nurseries for fish and invertebrates. *Bioscience*, *51*(8), 633–641. https://doi.org/10.1641/0006-3568(2001)051[0633:TICAMO]2.0.CO;2

Benner, P. A. (1992). Historical reconstruction of the Coquille River and surrounding landscape. In The action plan for Oregon coastal watersheds, estuaries, and ocean waters. Environmental Protection Agency Near Coastal Waters National Pilot Project 1988–91.

Brophy, L. S., Greene, C. M., Hare, V. C., Holycross, B., Lanier, A., Heady, W. N., et al. (2019). Insights into estuary habitat loss in the western United States using a new method for mapping maximum extent of tidal wetlands. *PLoS ONE*, *14*(8), e0218558. https://doi.org/10.1371/journal.pone.0218558

Burgette, R. J., Weldon, R. J., & Schmidt, D. A. (2009). Interseismic uplift rates for western Oregon and along-strike variation in locking on the Cascadia subduction zone. *Journal of Geophysical Research*, *114*, B01408. https://doi.org/10.1029/2008JB005679

Cahoon, D. R. (2006). A review of major storm impacts on coastal wetland elevations. *Estuaries and Coasts*, *29*(6), 889–898. https://doi.org/10.1007/BF02798648

Cahoon, D. R., Lynch, J. C., & Powell, A. N. (1996). Marsh vertical accretion in a Southern California estuary, USA. *Estuarine, Coastal and Shelf Science*, *43*(1), 19–32. https://doi.org/10.1006/ecss.1996.0055

Cahoon, D. R., & Reed, D. J. (1995). Relationships among marsh surface topography, hydroperiod, and soil accretion in a deteriorating Louisiana salt marsh. *Journal of Coastal Research*, *2*(43), 357–369. www.jstor.org/stable/4298345

Callaway, J. C., Borgnis, E. L., Turner, R. E., & Milan, C. S. (2012). Carbon sequestration and sediment accretion in San Francisco Bay tidal wetlands. *Estuaries and Coasts*, *35*(5), 1163–1181. https://doi.org/10.1007/s12237-012-9508-9

Callaway, J. C., Nyman, J. A., & DeLaune, R. D. (1996). Sediment accretion in coastal wetlands: A review and a simulation model of processes. *Current Topics in Wetland Biogeochemistry*, *2*, 2–23.

Castagno, K. A., Jiménez-Robles, A. M., Donnelly, J. P., Wiberg, P. L., Fenster, M. S., & Fagherazzi, S. (2018). Intense storms increase the stability of tidal bays. *Geophysical Research Letters*, *45*, 5491–5500. https://doi.org/10.1029/2018GL078208

Chmura, G. L. (2013). What do we need to assess the sustainability of the tidal salt marsh carbon sink? *Ocean and Coastal Management*, *83*, 25–31. https://doi.org/10.1016/j.ocecoaman.2011.09.006

Chmura, G. L., Anisfeld, S. C., Cahoon, D. R., & Lynch, J. C. (2003). Global carbon sequestration in tidal, saline wetland soils. *Global Biogeochemical Cycles*, *17*(4), 1111. https://doi.org/10.1029/2002GB001917

Chmura, G. L., Coffey, A., & Crago, R. (2001). Variation in surface sediment deposition on salt marshes in the Bay of Fundy. *Journal of Coastal Research*, *17*(1), 221–227.

Cochran, J. K., Frignani, M., Salamanca, M., Bellucci, L. G., & Guerzoni, S. (1998). Lead-210 as a tracer of atmospheric input of heavy metals in the northern Venice Lagoon. *Marine Chemistry*, *62*(1-2), 15–29. https://doi.org/10.1016/S0304-4203(98)00017-6

Colman, S. M., & Bratton, J. F. (2003). Anthropogenically induced changes in sediment and biogenic silica fluxes in Chesapeake Bay. *Geology*, *31*(1), 71–74. https://doi.org/10.1130/0091-7613(2003)031<0071:AICISA>2.0.CO;2

Conover, W. J. (1980). *Practical nonparametric statistics*, *Wiley series in probability and mathematical statistics. Applied probability and statistics* (2nd ed.). New York, NY: Wiley.

Cowardin, L. M., Carter, V., Golet, F. C., & LaRoe, E. T. (1979). Classification of wetlands and deepwater habitats of the United States. US Fish and Wildlife Service, Biological Services Program, Document FWS/OBS-79/31.

Craft, C. B., Seneca, E. D., & Broome, S. W. (1991). Loss on ignition and Kjeldahl digestion for estimating organic carbon and total nitrogen in estuarine marsh soils: Calibration with dry combustion. *Estuaries and Coasts*, *14*(2), 175–179. https://doi.org/10.2307/1351691

Crosby, S. C., Sax, D. F., Palmer, M. E., Booth, H. S., Deegan, L. A., Bertness, M. D., & Leslie, H. M. (2016). Salt marsh persistence is threatened by predicted sea-level rise. *Estuarine, Coastal and Shelf Science*, *181*(5), 93–99. https://doi.org/10.1016/j.ecss.2016.08.018

Davey, E., Wigand, C., Johnson, R., Sundberg, K., Morris, J., & Roman, C. T. (2011). Use of computed tomography imaging for quantifying coarse roots, rhizomes, peat, and particle densities in marsh soils. *Ecological Applications*, *21*(6), 2156–2171. https://doi.org/10.1890/10-2037.1

Day, J. W., Britsch, L. D., Hawes, S. R., Shaffer, G. P., Reed, D. J., & Cahoon, D. (2000). Pattern and process of land loss in the Mississippi Delta: A spatial and temporal analysis of wetland habitat change. *Estuaries and Coasts*, *23*(4), 425–438. https://doi.org/10.2307/1353136

DeLaune, R. D., Nyman, J. A., & Patrick, W. H. Jr. (1994). Peat collapse, ponding and wetland loss in a rapidly submerging coastal marsh. *Journal of Coastal Research*, *10*(4), 1021–1030.

Dicken, S. N., Johannessen, C., & Hanneson, B. (1961). Some recent physical changes of the Oregon coast. University of Oregon, Eugene, and Office of Naval Research, U.S. Department of the Navy Report NR 388-062.

Drexler, J. Z., Fuller, C. C., & Archfield, S. (2018). The approaching obsolescence of ^{137}Cs dating of wetland soils in North America. *Quaternary Science Reviews*, *199*, 83–96. https://doi.org/10.1016/j.quascirev.2018.08.028

Duarte, C. M., Losada, I. J., Hendriks, I. E., Mazarrasa, I., & Marbà, N. (2013). The role of coastal plant communities for climate change mitigation and adaptation. *Nature Climate Change*, *3*(11), 961–968. https://doi.org/10.1038/nclimate1970

Fagherazzi, S., Carniello, L., D'Alpaos, L., & Defina, A. (2006). Critical bifurcation of shallow microtidal landforms in tidal flats and salt marshes. *Proceedings of the National Academy of Sciences*, *103*(22), 8337–8341. https://doi.org/10.1073/pnas.0508379103

Fagherazzi, S., Kirwan, M. L., Mudd, S. M., Guntenspergen, G. R., Temmerman, S., D'Alpaos, A., et al. (2012). Numerical models of salt marsh evolution: Ecological, geomorphic, and climatic factors. *Reviews of Geophysics*, *50*, RG1102. https://doi.org/10.1029/2011RG000359

FitzGerald, D. M., Fenster, M. S., Argow, B. A., & Buynevich, I. V. (2008). Coastal impacts due to sea-level rise. *Annual Review of Earth and Planetary Sciences*, *36*, 601–647. https://doi.org/10.1146/annurev.earth.35.031306.140139

Foster, I. D., Mighall, T. M., Proffitt, H., Walling, D. E., & Owens, P. N. (2006). Post-depositional ^{137}Cs mobility in the sediments of three shallow coastal lagoons, SW England. *Journal of Paleolimnology*, *35*(4), 881–895. https://doi.org/10.1007/s10933-005-6187-6

Fourqurean, J., Johnson, B., Kauffman, J. B., Kennedy, H., & Lovelock, C. (2014). Field sampling of soil carbon pools in coastal ecosystems. In J. Howard, S. Hoyt, K. Isensee, E. Pidgeon, & M. Telszewski (Eds.), *Coastal blue carbon: Methods for assessing carbon stocks and emissions factors in mangroves, tidal salt marshes, and seagrass meadows* (pp. 39–66). Arlington, VA: Conservation International, Intergovernmental Oceanographic Commission of UNESCO, International Union for Conservation of Nature.

French, J. (2006). Tidal marsh sedimentation and resilience to environmental change: Exploratory modelling of tidal, sea-level and sediment supply forcing in predominantly allochthonous systems. *Marine Geology*, *235*(1-4), 119–136. https://doi.org/10.1016/j.margeo.2006.10.009

Friedrichs, C. T., & Perry, J. E. (2001). Tidal salt marsh morphodynamics: A synthesis. *Journal of Coastal Research*, *27*, 7–37. www.jstor.org/stable/25736162

Goñi, M. A., & Thomas, K. A. (2000). Sources and transformations of organic matter in surface soils and sediments from a tidal estuary (North Inlet, South Carolina, USA). *Estuaries*, *23*(4), 548–564. https://doi.org/10.2307/1353145

Goodbred, S. L. Jr., & Hine, A. C. (1995). Coastal storm deposition: Salt-marsh response to a severe extratropical storm, March 1993, west-central Florida. *Geology*, *23*(8), 679–682. https://doi.org/10.1130/0091-7613(1995)023<0679:CSDSMR>2.3.CO;2

Gunnell, J. R., Rodriguez, A. B., & McKee, B. A. (2013). How a marsh is built from the bottom up. *Geology*, *41*(8), 859–862. https://doi.org/10.1130/G34582.1

Heiri, O., Lotter, A. F., & Lemcke, G. (2001). Loss on ignition as a method for estimating organic and carbonate content in sediments: Reproducibility and comparability of results. *Journal of Paleolimnology*, *25*(1), 101–110. https://doi.org/10.1023/A:1008119611481

Hickey, B. M., & Banas, N. S. (2003). Oceanography of the US Pacific Northwest coastal ocean and estuaries with application to coastal ecology. *Estuaries*, *26*(4), 1010–1031. https://doi.org/10.1007/BF02803360

Holmquist, J. R., Windham-Myers, L., Bliss, N., Crooks, S., Morris, J. T., Megonigal, J. P., et al. (2018a). Accuracy and precision of tidal wetland soil carbon mapping in the conterminous United States. *Scientific Reports*, *8*(1), 9478. https://doi.org/10.1038/s41598-018-26948-7

Holmquist, J. R., Windham-Myers, L., Bliss, N., Crooks, S., Morris, J. T., Megonigal, J. P., et al. (2018b). Author Correction: Accuracy and precision of tidal wetland soil carbon mapping in the conterminous United States. *Scientific Reports*, *8*(1), 1–2. https://doi.org/10.1038/s41598-018-33283-4

Hood, W. G. (2004). Indirect environmental effects of dikes on estuarine tidal channels: Thinking outside of the dike for habitat restoration and monitoring. *Estuaries*, *27*(2), 273–282. https://doi.org/10.1007/BF02803384

IPCC (2013). In T. Hiraishi, T. Krug, K. Tanabe, N. Srivastava, J. Baasansuren, M. Fukuda, & T. G. Troxler (Eds.), *Supplement to the 2006 IPCC Guidelines for National Greenhouse Gas Inventories: Wetlands*. Switzerland: IPCC.

Janousek, C. N., Buffington, K. J., Thorne, K. M., Guntenspergen, G. R., Takekawa, J. Y., & Dugger, B. D. (2016). Potential effects of sea-level rise on plant productivity: Species-specific responses in northeast Pacific tidal marshes. *Marine Ecology Progress Series*, *548*, 111–125. https://doi.org/10.3354/meps11683

Janousek, C. N., & Folger, C. L. (2014). Variation in tidal wetland plant diversity and composition within and among coastal estuaries: Assessing the relative importance of environmental gradients. *Journal of Vegetation Science*, *25*(2), 534–545. https://doi.org/10.1111/jvs.12107

Janousek, C. N., Thorne, K. M., & Takekawa, J. Y. (2019). Vertical zonation and niche breadth of tidal marsh plants along the northeast Pacific coast. *Estuaries and Coasts*, *42*(1), 85–98. https://doi.org/10.1007/s12237-018-0420-9

Jefferson, C. A. (1975). Plant communities and succession in Oregon coastal salt marshes (Doctoral dissertation). Retrieved from ScholarsArchive@OSU. (https://ir.library.oregonstate.edu/concern/graduate_thesis_or_dissertations/2v23vx42t). Corvallis, OR: Oregon State University.

Kemp, A. C., Cahill, N., Engelhart, S. E., Hawkes, A. D., & Wang, K. (2018). Revising estimates of spatially variable subsidence during the AD 1700 Cascadia earthquake using a Bayesian foraminiferal transfer function. *Bulletin of the Seismological Society of America*, *108*(2), 654–673. https://doi.org/10.1785/0120170269

Kirwan, M. L., Guntenspergen, G. R., D'Alpaos, A., Morris, J. T., Mudd, S. M., & Temmerman, S. (2010). Limits on the adaptability of coastal marshes to rising sea level. *Geophysical Research Letters*, *37*, L23401. https://doi.org/10.1029/2010GL045489

Kirwan, M. L., Murray, A. B., Donnelly, J. P., & Corbett, D. R. (2011). Rapid wetland expansion during European settlement and its implication for marsh survival under modern sediment delivery rates. *Geology*, *39*(5), 507–510. https://doi.org/10.1130/G31789.1

Kirwan, M. L., Temmerman, S., Skeehan, E. E., Guntenspergen, G. R., & Fagherazzi, S. (2016). Overestimation of marsh vulnerability to sea level rise. *Nature Climate Change*, *6*(3), 253–260. http://doi.org/10.1038/nclimate2909

Kirwan, M. L., Walters, D. C., Reay, W. G., & Carr, J. A. (2016). Sea level driven marsh expansion in a coupled model of marsh erosion and migration. *Geophysical Research Letters*, *43*, 4366–4373. https://doi.org/10.1002/2016GL068507

Kolker, A. S., Goodbred, S. L., Hameed, S., & Cochran, J. K. (2009). High-resolution records of the response of coastal wetland systems to long-term and short-term sea-level variability. *Estuarine, Coastal and Shelf Science*, *84*(4), 493–508. https://doi.org/10.1016/j.ecss.2009.06.030

Komar, P. D., Allan, J. C., & Ruggiero, P. (2011). Sea level variations along the U.S. Pacific Northwest coast: Tectonic and climate controls. *Journal of Coastal Research*, *27*(5), 808–823. https://doi.org/10.2112/JCOASTRES-D-10-00116.1

MacKenzie, A. B., Hardie, S. M. L., Farmer, J. G., Eades, L. J., & Pulford, I. D. (2011). Analytical and sampling constraints in ^{210}Pb dating. *Science of the Total Environment*, *409*(7), 1298–1304. https://doi.org/10.1016/j.scitotenv.2010.11.040

Mariotti, G., & Fagherazzi, S. (2010). A numerical model for the coupled long-term evolution of salt marshes and tidal flats. *Journal of Geophysical Research*, *115*, F01004. https://doi.org/10.1029/2009JF001326

Mariotti, G., & Fagherazzi, S. (2013). Critical width of tidal flats triggers marsh collapse in the absence of sea-level rise. *Proceedings of the National Academy of Sciences*, *110*(14), 5353–5356. https://doi.org/10.1073/pnas.1219600110

Mazzotti, S., Jones, C., & Thomson, R. E. (2008). Relative and absolute sea level rise in western Canada and northwestern United States from a combined tide gauge-GPS analysis. *Journal of Geophysical Research*, *113*, C11019. https://doi.org/10.1029/2008JC004835

Mcleod, E., Chmura, G. L., Bouillon, S., Salm, R., Björk, M., Duarte, C. M., et al. (2011). A blueprint for blue carbon: Toward an improved understanding of the role of vegetated coastal habitats in sequestering CO^2. *Frontiers in Ecology and the Environment*, *9*(10), 552–560. https://doi.org/10.1890/110004

Milliman, J. D., & Syvitski, J. P. (1992). Geomorphic/tectonic control of sediment discharge to the ocean: The importance of small mountainous rivers. *The Journal of Geology*, *100*(5), 525–544. https://doi.org/10.1086/629606

Mitchell, C. E., Vincent, P., Weldon, R. J., & Richards, M. A. (1994). Present-day vertical deformation of the Cascadia Margin, Pacific Northwest, United States. *Journal of Geophysical Research*, *99*(B6), 12,257–12,277. https://doi.org/10.1029/94JB00279

Morris, J. T., Barber, D. C., Callaway, J. C., Chambers, R., Hagen, S. C., Hopkinson, C. S., et al. (2016). Contributions of organic and inorganic matter to sediment volume and accretion in tidal wetlands at steady state. *Earth's Future*, *4*(4), 110–121. http://doi.org/10.1002/2015EF000334

Morris, J. T., Sundareshwar, P. V., Nietch, C. T., Kjerfve, B., & Cahoon, D. R. (2002). Responses of coastal wetlands to rising sea level. *Ecology*, *83*(10), 2869–2877. https://doi.org/10.1890/0012-9658(2002)083[2869:ROCWTR]2.0.CO;2

Mudd, S. M., Howell, S. M., & Morris, J. T. (2009). Impact of dynamic feedbacks between sedimentation, sea-level rise, and biomass production on near-surface marsh stratigraphy and carbon accumulation. *Estuarine, Coastal and Shelf Science*, *82*(3), 377–389. https://doi.org/10.1016/j.ecss.2009.01.028

Mustaphi, C. J. C., Brahney, J., Aquino-Lopez, M. A., Goring, S., Orton, K., Noronha, A., et al. (2019). Guidelines for reporting and archiving ^{210}Pb sediment chronologies to improve fidelity and extend data lifecycle. *Quaternary Geochronology*, *52*, 77–87. https://doi.org/10.1016/j.quageo.2019.04.003

Nevissi, A. E. (1985). Measurement of ^{210}Pb atmospheric flux in the Pacific Northwest. *Health Physics*, *48*(2), 169–174. http://doi.org/10.1097/00004032-198502000-00003

Ouyang, X., & Lee, S. Y. (2014). Updated estimates of carbon accumulation rates in coastal marsh sediments. *Biogeosciences*, *11*, 5057–5071. https://doi.org/10.5194/bg-11-5057-2014

Pendleton, L., Donato, D. C., Murray, B. C., Crooks, S., Jenkins, W. A., Sifleet, S., et al. (2012). Estimating global "blue carbon" emissions from conversion and degradation of vegetated coastal ecosystems. *PLoS ONE*, *7*(9), e43542. https://doi.org/10.1371/journal.pone.0043542

Redfield, A. C. (1972). Development of a New England salt marsh. *Ecological Monographs*, *42*(2), 201–237. https://doi.org/10.2307/1942263

Reed, D. J. (1989). Patterns of sediment deposition in subsiding coastal salt marshes, Terrebonne Bay, Louisiana: The role of winter storms. *Estuaries*, *12*(4), 222–227. https://doi.org/10.2307/1351901

Reed, D. J. (1995). The response of coastal marshes to sea-level rise: Survival or submergence? *Earth Surface Processes and Landforms*, *20*(1), 39–48. https://doi.org/10.1002/esp.3290200105

Ritchie, J. C., & McHenry, J. R. (1990). Application of radioactive fallout cesium-137 for measuring soil erosion and sediment accumulation rates and patterns: A review. *Journal of Environmental Quality*, *19*(2), 215–233. http://doi.org/10.2134/jeq1990.00472425001900020006x

Roner, M., D'Alpaos, A., Ghinassi, M., Marani, M., Silvestri, S., Franceschinis, E., & Realdon, N. (2016). Spatial variation of salt-marsh organic and inorganic deposition and organic carbon accumulation: Inferences from the Venice lagoon, Italy. *Advances in Water Resources*, *93*(B), 276–287. https://doi.org/10.1016/j.advwatres.2015.11.011

Sanchez-Cabeza, J. A., & Ruiz-Fernández, A. C. (2012). ^{210}Pb sediment radiochronology: An integrated formulation and classification of dating models. *Geochimica et Cosmochimica Acta*, *82*(1), 183–200. https://doi.org/10.1016/j.gca.2010.12.024

Schile, L. M., Callaway, J. C., Morris, J. T., Stralberg, D., Parker, V. T., & Kelly, M. (2014). Modeling tidal marsh distribution with sea-level rise: Evaluating the role of vegetation, sediment, and upland habitat in marsh resiliency. *PLoS ONE*, *9*(2), e88760. https://doi.org/10.1371/journal.pone.0088760

Schuerch, M., Vafeidis, A., Slawig, T., & Temmerman, S. (2013). Modeling the influence of changing storm patterns on the ability of a salt marsh to keep pace with sea level rise. *Journal of Geophysical Research: Earth Surface*, *118*, 84–96. https://doi.org/10.1029/2012JF002471

Stoddart, D. R., Reed, D. J., & French, J. R. (1989). Understanding salt-marsh accretion, Scolt Head Island, Norfolk, England. *Estuaries*, *12*(4), 228–236. https://doi.org/10.2307/1351902

Swanson, K. M., Drexler, J. Z., Schoellhamer, D. H., Thorne, K. M., Casazza, M. L., Overton, C. T., et al. (2014). Wetland Accretion Rate Model of Ecosystem Resilience (WARMER) and its application to habitat sustainability for endangered species in the San Francisco Estuary. *Estuaries and Coasts*, *37*(2), 476–492. https://doi.org/10.1007/s12237-013-9694-0

Taylor, J. R. (1997). *An introduction to error analysis: The study of uncertainties in physical measurements* (2nd ed.). Sausalito, CA: University Science Books.

Temmerman, S., Govers, G., Meire, P., & Wartel, S. (2003). Modelling long-term tidal marsh growth under changing tidal conditions and suspended sediment concentrations, Scheldt estuary, Belgium. *Marine Geology*, *193*(1-2), 151–169. https://doi.org/10.1016/S0025-3227(02)00642-4

Thom, R. M. (1992). Accretion rates of low intertidal salt marshes in the Pacific Northwest. *Wetlands*, *12*(3), 147–156. https://doi.org/10.1007/BF03160603

Thom, R. M., & Borde, A. B. (1998). Human intervention in Pacific Northwest coastal ecosystems. In G. R. McMurray & R. J. Bailey (Eds.), *Change in Pacific Northwest coastal ecosystems* (pp. 5–37). Silver Spring, MD: NOAA Coastal Ocean Program, Decision Analysis Series.

Thorne, K., MacDonald, G., Guntenspergen, G., Ambrose, R., Buffington, K., Dugger, B., et al. (2018). US Pacific coastal wetland resilience and vulnerability to sea-level rise. *Science Advances*, *4*(2), eaao3270. https://doi.org/10.1126/sciadv.aao3270

Thorne, K. M., Elliott-Fisk, D. L., Wylie, G. D., Perry, W. M., & Takekawa, J. Y. (2014). Importance of biogeomorphic and spatial properties in assessing a tidal salt marsh vulnerability to sea-level rise. *Estuaries and Coasts*, *37*(4), 941–951. https://doi.org/10.1007/s12237-013-9725-x

Turner, A., & Millward, G. E. (2002). Suspended particles: their role in estuarine biogeochemical cycles. *Estuarine, Coastal and Shelf Science*, *55*(6), 857–883. https://doi.org/10.1006/ecss.2002.1033

Turner, R. E., Baustian, J. J., Swenson, E. M., & Spicer, J. S. (2006). Wetland sedimentation from Hurricanes Katrina and Rita. *Science*, *314*(5798), 449–452. http://doi.org/10.1126/science.1129116

Tweel, A. W., & Turner, R. E. (2014). Contribution of tropical cyclones to the sediment budget for coastal wetlands in Louisiana, USA. *Landscape Ecology*, *29*(6), 1083–1094. https://doi.org/10.1007/s10980-014-0047-6

van Ardenne, L. B., Jolicouer, S., Bérubé, D., Burdick, D., & Chmura, G. L. (2018). The importance of geomorphic context for estimating the carbon stock of salt marshes. *Geoderma*, *330*(15), 264–275. https://doi.org/10.1016/j.geoderma.2018.06.003

Watson, E. B., Wigand, C., Davey, E. W., Andrews, H. M., Bishop, J., & Raposa, K. B. (2017). Wetland loss patterns and inundation-productivity relationships prognosticate widespread salt marsh loss for southern New England. *Estuaries and Coasts*, *40*(3), 662–681. https://doi.org/10.1007/s12237-016-0069-1

Weston, N. B. (2014). Declining sediments and rising seas: an unfortunate convergence for tidal wetlands. *Estuaries and Coasts*, *37*(1), 1–23. https://doi.org/10.1007/s12237-013-9654-8

Wheatcroft, R. A., Goñi, M. A., Richardson, K. N., & Borgeld, J. C. (2013). Natural and human impacts on centennial sediment accumulation patterns on the Umpqua River margin, Oregon. *Marine Geology*, *339*(1), 44–56. https://doi.org/10.1016/j.margeo.2013.04.015

Wheatcroft, R. A., & Sommerfield, C. K. (2005). River sediment flux and shelf sediment accumulation rates on the Pacific Northwest margin. *Continental Shelf Research*, *25*(3), 311–332. https://doi.org/10.1016/j.csr.2004.10.001

Wheatcroft, R. A., Stevens, A. W., Hunt, L. M., & Milligan, T. G. (2006). The large-scale distribution and internal geometry of the fall 2000 Po River flood deposit: Evidence from digital X-radiography. *Continental Shelf Research*, *26*(4), 499–516. https://doi.org/10.1016/j.csr.2006.01.002

Wiberg, P. L., Fagherazzi, S., & Kirwan, M. L. (2020). Improving predictions of salt marsh evolution through better integration of data and models. *Annual Review of Marine Science*, *12*, 389–413. https://doi.org/10.1146/annurev-marine-010419-010610

Windham-Myers, L., Crooks, S., & Troxler, T. G. (Eds.) (2019). *A blue carbon primer: The state of coastal wetland carbon science, practice, and policy*. Boca Raton, FL: Taylor & Francis Group.

Wise, D. R. (2018). Updates to the suspended sediment SPARROW model developed for western Oregon and northeastern California. U.S. Geological Survey Scientific Investigations Report 2018–5156. https://doi.org/10.3133/sir20185156

Wise, D. R., & O'Connor, J. E. (2016). A spatially explicit suspended-sediment load model for western Oregon. U.S. Geological Survey Scientific Investigations Report 2016–5079. https://doi.org/10.3133/sir20165079